SCIENTIFIC REPORTS

OPEN

Asymmetric magnetic proximity effect in a Pd/Co/Pd trilayer system

Dong-Ok Kim[1,2], Kyung Mee Song[2,3], Yongseong Choi[4], Byoung-Chul Min[2], Jae-Sung Kim[3], Jun Woo Choi[2] & Dong Ryeol Lee[1,4]

Received: 14 January 2016
Accepted: 15 April 2016
Published: 06 May 2016

In spintronic devices consisting of ferromagnetic/nonmagnetic systems, the ferromagnet-induced magnetic moment in the adjacent nonmagnetic material significantly influences the spin transport properties. In this study, such magnetic proximity effect in a Pd/Co/Pd trilayer system is investigated by x-ray magnetic circular dichroism and x-ray resonant magnetic reflectivity, which enables magnetic characterizations with element and depth resolution. We observe that the total Pd magnetic moments induced at the top Co/Pd interface are significantly larger than the Pd moments at the bottom Pd/Co interface, whereas transmission electron microscopy and reflectivity analysis indicate the two interfaces are nearly identical structurally. Such asymmetry in magnetic proximity effects could be important for understanding spin transport characteristics in ferromagnetic/nonmagnetic systems and its potential application to spin devices.

Spin transport in ferromagnet/nonmagnetic metal (FM/NM) systems have been extensively studied. Interfacial spin-orbit coupling in such systems leads to interesting spin related phenomena and interactions, at the same time providing an effective pathway for electrical manipulation of the magnetization[1–13]. The spin Hall effect (SHE)[14–19] in the FM/NM system, in which a charge current in the NM layer produces a spin current into the FM, can be used for reversible magnetization switching of the FM layer[7–8]. Current induced spin-orbit torques (SOT) originating from strong interfacial spin-orbit coupling at the FM/NM interface also enables efficient magnetization switching[3]. The interfacial Dzyaloshinskii-Moriya interaction (DMI)[20,21] in FM/NM systems, together with the SHE effect, leads to asymmetric field driven domain wall motion (DWM) and high velocity current-driven DWM[9,10,22–25]. In certain FM/NM systems (e.g. Co/Pt, Fe/Pd), the ferromagnet induces a magnetic moment in the adjacent nonmagnetic material due to the magnetic proximity effect[26–33]. The magnetic proximity effect must be carefully considered in spin transport measurements since the induced magnetic moment significantly influences spin transport in such systems. Recent studies reveal that the magnetic proximity effect results in modifications to spin transport phenomena such as increased current-driven DWM velocity, reduced SHE, and occurrence of the anomalous Nernst effect[25,31,32,34–38]. The magnetic properties of the atoms near the FM/NM interface are important for understanding the interface sensitive magnetic proximity effect. Theoretical and experimental studies also suggest that structural properties of the FM and NM atoms near the interface play a prominent role in determining the spin transport properties[39,40]. Therefore, it is important to investigate the structural and magnetic properties at the interface to better understand the spin transport properties of the FM/NM systems.

One interesting aspect of the ferromagnet/nonmagnetic metal systems is the non-equivalent spin transport properties (e.g. SOT, DMI) between NM/FM (FM on top of NM) and FM/NM (NM on top of FM) systems, which has been attributed to the broken spatial inversion symmetry at the FM-NM interface[40]. Even in a symmetric NM/FM/NM structure, the inversion symmetry could be broken if the structural and magnetic properties of the bottom NM/FM and top FM/NM layers are not identical. Earlier studies show that the SOT and DMI do not necessarily cancel out in symmetric NM/FM/NM structures, implying that the structural and/or magnetic properties at the bottom NM/FM and top FM/NM interfaces are distinct. Although the structural difference between the top and bottom interfaces in a NM/FM/NM structure have been observed experimentally, distinguishing possible asymmetry in magnetic properties between the two interfaces has been not trivial. Measuring magnetic properties at the two interfaces separately requires element- and depth-resolved magnetic characterization. In particular, magnetic depth profiles of magnetically induced 4*d* transition metals (e.g. Pd) have been lacking due

[1]Department of Physics, Soongsil University, Seoul 06978, Republic of Korea. [2]Center for Spintronics, Korea Institute of Science and Technology, Seoul 02792, Republic of Korea. [3]Department of Physics, Sookmyung Women's University, Seoul 04130, Republic of Korea. [4]Advanced Photon Source, Argonne National Laboratory, Argonne, Illinois 60439, USA. Correspondence and requests for materials should be addressed to J.W.C. (email: junwoo@kist.re.kr) or D.R.L. (email: drlee@ssu.ac.kr)

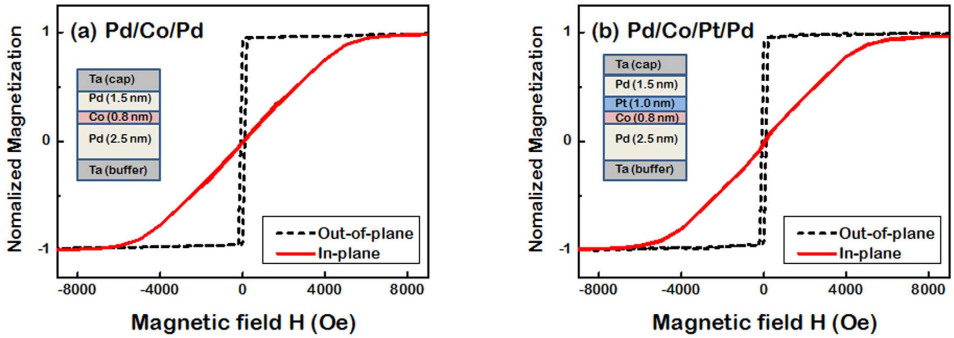

Figure 1. Magnetic hysteresis loops of (**a**) Pd/Co/Pd and (**b**) Pd/Co/Pt/Pd samples measured by VSM. Despite the insertion of the 1 nm thick Pt film between the Co and top Pd, the magnetic hysteresis loops of the two samples are almost identical with a strong perpendicular magnetic anisotropy.

to the dearth of magnetic scattering beamlines with x-ray energies near the 4*d* transition metal *L* edges (~3 keV). In this study, the depth profiles of the structural and magnetic properties in a NM/FM/NM trilayer system (Pd/Co/Pd) are investigated using x-ray magnetic circular dichroism and x-ray resonant magnetic reflectivity. While the top and bottom interfaces appear to have an almost identical structure, we observe a difference in the induced magnetic moment between the top and bottom NM (Pd). The top NM (Pd) was found to have a significantly thicker "magnetically induced" region and a larger total induced magnetic moment compared to those of the bottom NM (Pd).

Results

Two separate sets of Pd/Co/Pd thin film structures are selected to study the magnetic proximity effect: (i) Si/SiO_2/Ta(5)/Pd(2.5)/Co(0.8)/Pd(1.5)/Ta(3) [hereafter referred to as Pd/Co/Pd] and (ii) Si/SiO_2/Ta(5)/Pd(2.5)/Co(0.8)/Pt(1)/Pd(1.5)/Ta(3) [hereafter referred to as Pd/Co/Pt/Pd]; the number in parenthesis is the nominal film thickness in nm. A 1 nm thick Pt film is inserted between the Co and top Pd in the Pd/Co/Pt/Pd in order to suppress the induced magnetism in the top Pd while not significantly altering the magnetic anisotropy. The magnetic characterization by vibrating sample magnetometry (VSM) shows that both samples have strong perpendicular magnetic anisotropy (Fig. 1). Despite the insertion of a 1 nm thick Pt film between the Co and top Pd in Pd/Co/Pt/Pd, the magnetic hysteresis loops of the two samples are almost identical with out-of-plane magnetic easy axes and large in-plane magnetic saturation fields of ~6 kOe. Both Co-Pd and Co-Pt interfaces are known to have a strong interfacial perpendicular magnetic anisotropy[41–45].

The microstructure of Pd/Co/Pd is investigated by high resolution transmission electron microscopy (HRTEM) and scanning transmission electron microscopy (STEM). The HRTEM image (Fig. 2(a)) reveals that the Pd/Co/Pd film is highly textured on top of an amorphous Ta buffer layer. Although the fast Fourier transform (FFT) indicates that the Pd/Co/Pd has an overall (111) texture, the sporadic dark regions in between the textured region suggest that the Pd/Co/Pd is likely multi-grained. The contrast in the STEM (Fig. 2(b)) is sensitive to the atomic number so that the Co, Pd, and Ta layers are more clearly distinguished. Note that despite a large fraction of the capping Ta layer being oxidized, a thin metallic Ta layer exists between the TaOx and the top Pd that prevents the oxidation of the Pd. Figure 2(c) shows the elemental distribution in the Pd/Co/Pd structure acquired from the energy-dispersive x-ray (EDX) spectrum along the film normal direction. Considerable Ta-Pd and Co-Pd interfacial roughness exists throughout the Ta/Pd/Co/Pd/Ta interfaces. Nevertheless, the Co and Pd films can be clearly distinguished in the STEM image and EDX spectrum.

In order to clearly quantify and distinguish the structural properties (interfacial roughness, density profile, etc.) of the bottom Pd/Co and top Co/Pd interfaces in Pd/Co/Pd, resonant x-ray reflectivity (RXR) were measured at the Pd L_3 edge. RXR is an experimental technique in which the x-ray reflectivity is measured at the absorption edge of a specific element[46]. X-ray reflectivity is widely used to determine the laterally averaged depth profile at the sub-nanometer scale for the total film structure; RXR is an advantageous choice for obtaining a depth profile specific to a certain element, since the atomic scattering factors are dramatically changed around the absorption edge of the specific element of interest. The comparison of the reflectivity intensities measured at the absorption edge and away from the absorption edge can provide an element specific contrast in the total atomic scattering factors, which is then used for obtaining an element specific depth profile (See Supplementary information). The x-ray reflectivity of the Pd/Co/Pd is measured at the Pd L_3 edge (E = 3.174 keV) and away from the Pd L_3 edge (E = 3.160 keV) as shown in Fig. 3(a). The reflected intensities are normalized by the Fresnel reflection R_F from the ideally smooth Si surface to emphasize the interference patterns due to the film structures. The electronic density profiles are determined from the simultaneous fitting of the two x-ray reflectivity curves in Fig. 3(a). (See Supplementary information) The x-ray reflectivity curves are fitted with multiple parameters such as the film thickness, film density, and interfacial roughness of each layer. The solid lines in Fig. 3(a) represents the calculated x-ray reflectivity based on the best fit model. The interpretation of this data provides a total refractive index profile proportional to the electronic density (Fig. 3(b)), revealing the element-specific depth profile of the elements. Because the x-ray atomic factor of the Pd is the only parameter that could result in the different density profiles between E = 3.174 keV and 3.160 keV, the contrast in the density profiles (dash-dotted blue lines in Fig. 3(b)) corresponds to the element-specific depth profile of the Pd films.

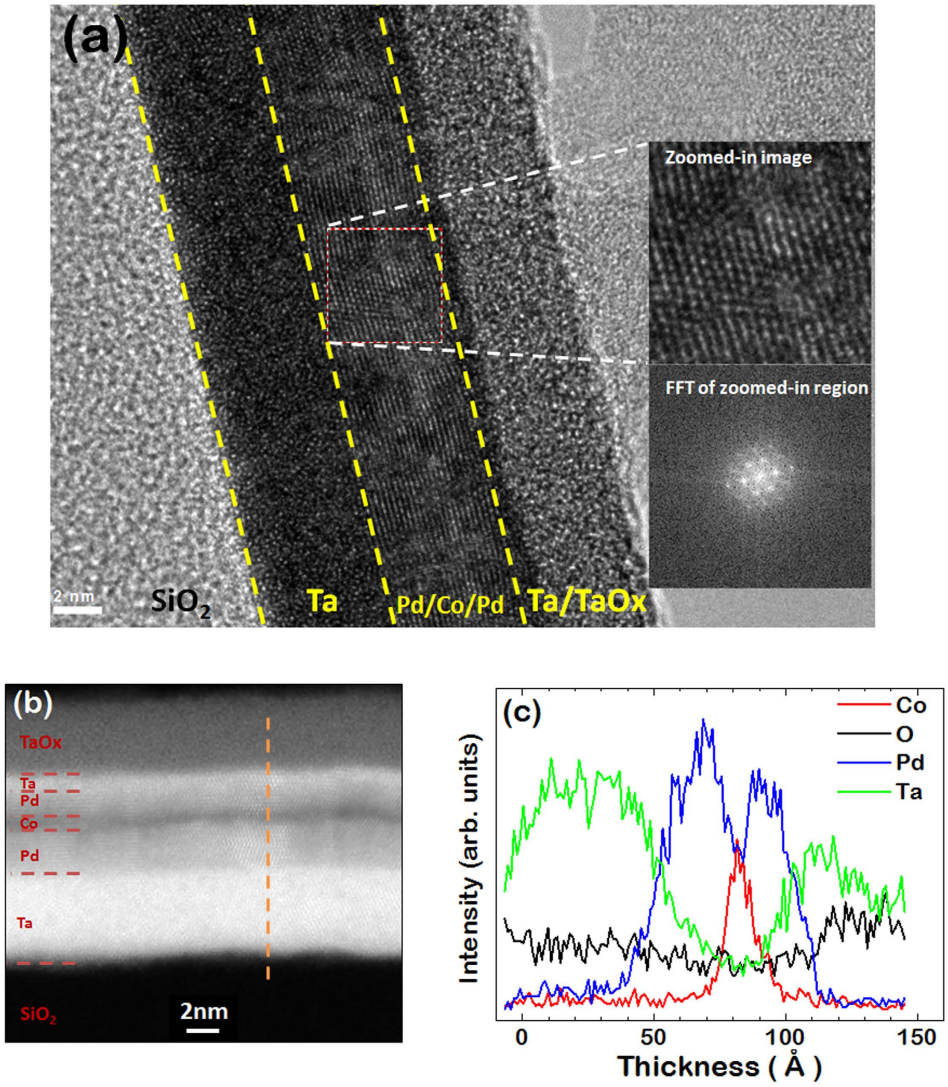

Figure 2. (**a**) TEM image of the Ta/Pd/Co/Pd/Ta film. The zoomed-in image and its FFT show that the Pd/Co/Pd trilayer is epitaxial with an fcc (111) texture. (**b**) STEM image of the Ta/Pd/Co/Pd/Ta film. (**c**) EDX spectra along the orange dotted line in (**b**).

The RXR also provides information about the interfacial roughness in Pd/Co/Pd. The measure of interfacial roughness at the Pd/Co and Co/Pd interfaces are defined as $w_{Pd/Co}$ and $w_{Co/Pd}$, respectively, as depicted in Fig. 3(c). In the best fit model, the interfacial roughness at the bottom Pd/Co interface $w_{Pd/Co}$ (2.8 Å) and the top Co/Pd interface $w_{Co/Pd}$ (2.6 Å) are found to be nearly identical. To check the validity of the best fit, reflectivity calculations based on models with different interfacial roughness at the Pd/Co and Co/Pd interfaces are plotted as dashed and dotted lines in Fig. 3(a). The contrast is remarkable at the Pd L_3 edge (E = 3.174 keV), where the reflectivity curves of other models (dashed and dotted lines in the bottom panel of Fig. 3(a)) with asymmetric interfacial roughness clearly show deviations from the experimental data. The deviations are prominent at high q_z's, whose corresponding length scales are close to the interfacial roughness. Clear deviations between the measured reflectivity and the dashed and dotted lines in Fig. 3(a) demonstrate the high sensitivity of the RXR on the fitting models. Because the RXR curves are best fitted with the structural model with nearly identical (2.6 Å~2.8 Å) interfacial roughness at the top and bottom Pd-Co interface, it is certain that there is little difference in interfacial roughness between the bottom Pd/Co and top Co/Pd interfaces.

For element specific magnetic characterizations, the induced magnetic moments of Pd and Pt are measured by fluorescence detected x-ray magnetic circular dichroism (XMCD) with right and left circularly polarized x-rays tuned to the Pd and Pt *L* edges (Fig. 4). XMCD provides direct proof of the magnetic proximity effect by element specific measurement of the induced magnetic moments of nonmagnetic elements in contact with ferromagnetic materials[27–30,32,33]. An incident x-ray angle of 3.6 degrees was chosen to maximize the probing volume (due to the larger footprint at grazing angles) and subsequently magnetic sensitivity. The measurements were done with the maximum in-plane magnetic field of ~5 kOe, since XMCD is mostly sensitive to the magnetic moment along the x-ray propagation direction (nearly in-plane at grazing incidence). Although the Pd/Co/Pd and Pd/Co/Pt/Pd

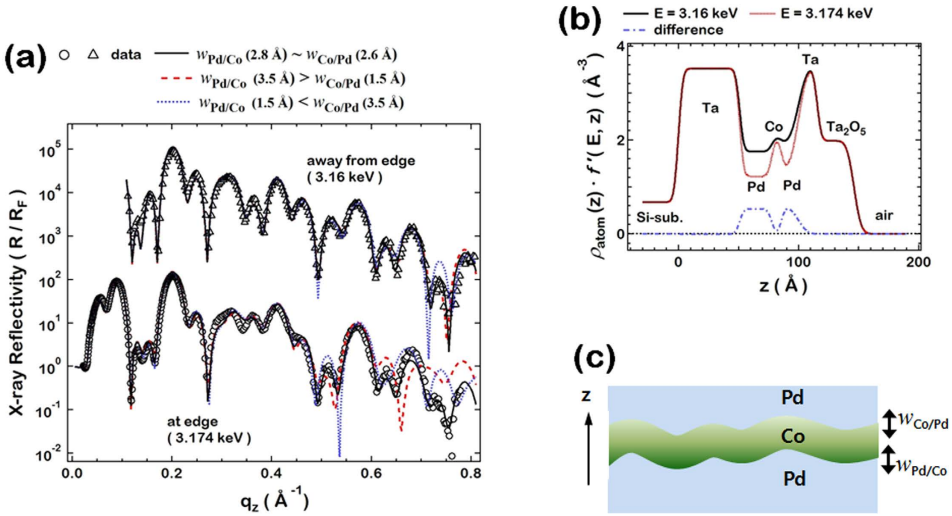

Figure 3. (**a**) X-ray reflectivity intensities measured at the resonant (3.174 keV) and non-resonant (3.16 keV) energies. The reflected intensities were normalized by the Fresnel reflection R_F from the ideally smooth Si surface. q_z is defined as $(4\pi/\lambda)\sin\theta$ where θ and λ are the angle and wavelength of the incident x-ray. (**b**) Electronic density profiles determined from the best fits for the resonant and non-resonant energies. The difference between the two data is proportional to the density profile of the Pd layers. (**c**) The interfacial roughness at the Pd/Co and Co/Pd interfaces are defined as $w_{Pd/Co}$ and $w_{Co/Pd}$, respectively.

films have perpendicular magnetic anisotropy, a large in-plane field rotates the magnetization towards the in-plane direction. The nearly equivalent in-plane magnetic hysteresis loops of the two samples imply that the magnetization directions of the two samples are almost identical with an applied in-plane field of ~5 kOe. The Pd L_2 edge could not be measured due to the overlap with the Ar K edge of the ambient Ar gas in the x-ray path leading up to the sample. The lack of the XMCD data at the Pd L_2 edge prevents us from exactly quantifying the Pd magnetic moment using the XMCD sum rule. The incident x-ray angle of 3.6 degrees ensures that the Pd XMCD measurement probes both of the Pd layers. The path length of the incident x-ray at this angle within any layer (tens of nm) is much smaller than the x-ray absorption length for the layer across the Pd L_3 edge (hundreds of nm). Similarly, the total film thickness (<10 nm) is much smaller than the x-ray absorption length for the emitted Pd L_α fluorescence which is at least a few hundreds of nm for any layers. Therefore, contributions from the top and bottom Pd to the measured Pd magnetic signal would be nearly identical if the induced magnetic moments of the two Pd films were equivalent in Pd/Co/Pd.

The XMCD intensities, normalized by the averaged x-ray absorption spectroscopy (XAS) intensities at the energies above the Pd L_3 absorption edge, are shown in Fig. 4(a),(b). The peak of the XMCD spectra is −4.7% and −1.9% for Pd/Co/Pd and Pd/Pt/Co/Pd, respectively. The decrease of the XMCD signal in Pd/Pt/Co/Pd compared to Pd/Co/Pd is not unexpected since the 1 nm thick Pt film inserted between the top Pd and Co would reduce the induced magnetic moment of the top Pd. The XMCD peak of Pd/Co/Pt/Pd should be the half of that of Pd/Co/Pd (i.e. −2.35%) in the extreme case that there is no magnetic moment induced in the top Pd in Pd/Co/Pt/Pd due to the inserted 1 nm thick Pt. The magnetic moment of Pd/Co/Pt/Pd (−1.9%) is even less than the half of that of Pd/Co/Pd, implying that the top Pd magnetic moment in the Pd/Co/Pd is larger than the bottom Pd magnetic moment in the Pd/Co/Pd. Pt is an element also known to have the magnetic proximity effect which is confirmed by the XMCD at the Pt L_2 edge in Fig. 4(c). In earlier studies the Pt magnetic proximity effect remains up to ~1 nm from the ferromagnetic interface[28,29], so that it is possible that the 1 nm thick Pt film does not completely eliminate the magnetic proximity effect of Pd. If a non-zero magnetic moment exists in the top Pd of the Pd/Co/Pt/Pd, the asymmetry of the induced magnetic moment between the top and bottom Pd would be even larger. From this, it is certain that the top Pd magnetic moment in the Pd/Co/Pd is larger than the bottom Pd magnetic moment.

To confirm the XMCD results that the top Pd has a larger magnetic moment, x-ray resonant magnetic reflectivity (XRMR) of the Pd/Co/Pd was measured. Similar to RXR, which revealed the structural depth profile of the Pd, XRMR analysis can be utilized to determine the depth profile of the induced magnetic moments of Pd atoms. XRMR has been successfully utilized for determination of the laterally averaged depth profile of element specific magnetic moments[47,48] (See Supplementary information). While soft x-ray XRMR has been used to investigate interface magnetism of 3d ferromagnetic materials[49,50], intermediate energy x-ray was used in this study to measure the interface magnetism of Pd, a 4d metal. For XRMR analysis of the Pd/Co/Pd sample, the scattering intensity of the right (I_+) and left (I_-) circularly polarized incident x-rays at the Pd L_3 edge was measured while applying an in-plane magnetic field of ~5 kOe. It should be noted that in the grazing incidence measurement geometry of the intermediate x-ray XRMR done in our experiments, only the in-plane magnetization would be measureable, since the large angle between the surface normal (perpendicular direction) and the x-ray beam direction would result in small magnetic contrast for perpendicular magnetization. Therefore, all the magnetic x-ray measurements were done with the maximum in-plane magnetic field of ~5 kOe.

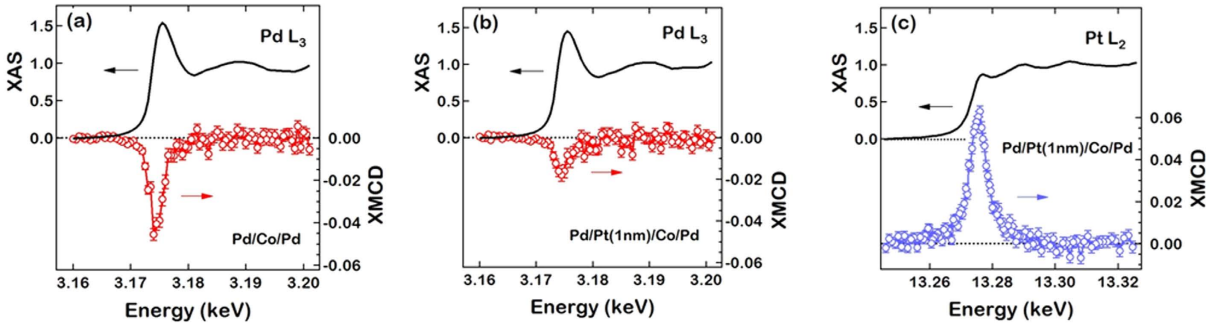

Figure 4. XAS and XMCD measured from the samples Pd/Co/Pd (**a**) and Pd/Pt/Co/Pd (**b,c**). The photon energies of circularly polarized x-rays were tuned to the Pd L_3 (**a,b**) and Pt L_2 (**c**) edges to extract element-specific information of the induced magnetic moments of Pd and Pt atoms, respectively. The XAS and XMCD intensities were normalized by the averaged XAS intensities over the energies above the absorption edge. It should be noted the overlap of the Ar *K* edge with the Pd L_2 edge prevents measurement of the XAS and XMCD intensities at the Pd L_2 edge. Similarly the interference between the Ta L_β and Pt L_α fluorescence lines was too strong to measure at the Pt L_3 edge.

The Pd magnetic moments is proportional to the asymmetry ratio, $(I_+ - I_-)/(I_+ + I_-)$, which is defined as the difference in the scattering intensity divided by the sum, shown in the bottom panel of Fig. 5(a). The x-ray reflectivity shown in the top panel in Fig. 5(a) is only sensitive to the structure (electronic density). The asymmetry ratio is fitted with various "magnetic models" to determine the magnetic depth profile. In these models, it is assumed that there are regions of Pd with induced magnetic moments in proximity to Co, and regions of non-magnetic Pd far away from the Co interface, shown schematically in Fig. 5(b). The "magnetic thickness" of Pd is the spatial extent of the region in which Pd has induced magnetic moments. There also exists a magnetic interface region between the magnetic Pd and its adjacent layers, with an accompanying "magnetic interface roughness". There are four such interfaces which are depicted as dashed and dotted lines in Fig. 5(b): the two nonmagnetic/magnetic interfaces in the top and bottom Pd, and the two Co-Pd interfaces. We also define the magnetic amplitudes $m_{\mathrm{Pd}}^{\mathrm{top}}$ and $m_{\mathrm{Pd}}^{\mathrm{bot}}$, which are the scaling factors for the Pd magnetic moments in the top and bottom Pd magnetic regions, respectively; the estimation of the absolute quantity of the magnetic moment is discussed in the Supplementary information.

In order to understand the asymmetric magnetic moments between the top and bottom Pd layers observed in the XMCD, we assume two magnetic models of the induced Pd magnetic moments: (1) the Pd magnetic layers for the top and bottom Pd layers have identical magnetic amplitudes, $m_{\mathrm{Pd}}^{\mathrm{top}} = m_{\mathrm{Pd}}^{\mathrm{bot}}$, but different magnetic layer thicknesses, $d_{mag}^{top} \neq d_{mag}^{bot}$ (model A in Figs 5(b) and (2)) identical magnetic layer thicknesses, $d_{mag}^{top} = d_{mag}^{bot}$, but different magnetic amplitudes, $m_{\mathrm{Pd}}^{\mathrm{top}} \neq m_{\mathrm{Pd}}^{\mathrm{bot}}$ (model B in Fig. 5(b)). The best fit (solid lines in Fig. 5(a)) using model A shows good agreement with the experimental data. In the best fit model, the magnetic amplitude of the magnetic layers is found to be 1.0(±0.1), and the magnetic layer thicknesses are 2.7(±0.2) Å and 6.9(±0.3) Å for the bottom and top Pd layers, respectively. The magnetic interface roughnesses at the purely magnetic interfaces (magnetic Pd-nonmagnetic Pd) are found to be 1.5(±0.2) Å and 3.8(±0.3) Å for the bottom and top Pd layers, respectively. These fitting results indicate that the top and bottom Pd layers have asymmetric magnetic thicknesses and asymmetric magnetic interface roughnesses, with the thicker top Pd magnetic layer having a rougher magnetic interface.

To verify the validity of the asymmetric magnetic roughnesses determined from the best fit, we plot the calculated asymmetry ratios from other models (including model B) in Fig. 5(a), the details of which are discussed in the Supplementary information. The drastic change in the calculated asymmetry ratio with various models clearly shows the sensitivity of XRMR on the magnetic depth profiles; this sensitivity implies that the best fit model may well represent the actual magnetic depth profile. The Pd magnetic depth profile from the best fit model is plotted in Fig. 5(c) overlapped with the elemental electronic density profile normalized by the bulk value. (See Supplementary information) The area of the gray region ($\mathrm{Pd}_{\mathrm{magnetic}}$) in Fig. 5(c) depicts the total integrated magnetic moment of the Pd atoms. The top Pd layer has a thicker magnetic region (width of the gray region) and larger total integrated magnetic moment (area of the gray region) which explains why the top Pd shows a larger magnetic signal in the XMCD experiments. It is evident that the top and bottom Pd films show asymmetry in the magnetic thickness and total magnetic moment.

Discussion

We present two possible origins of the asymmetric magnetic proximity effect of Pd observed in this study. First, it should be noted that the top and bottom Pd thicknesses in the Pd/Co/Pd sample, 1.5 nm and 2.5 nm, respectively, are different. Theoretical studies predict a thickness dependent magnetic moment of a Pd film[51], so that the difference in top and bottom Pd thicknesses could result in different Pd magnetic moments. A systematic Pd thickness dependent study of the Pd magnetic moments in the Pd/Co/Pd structure might be needed in the future to investigate whether the Pd thickness is indeed responsible for the observed asymmetry.

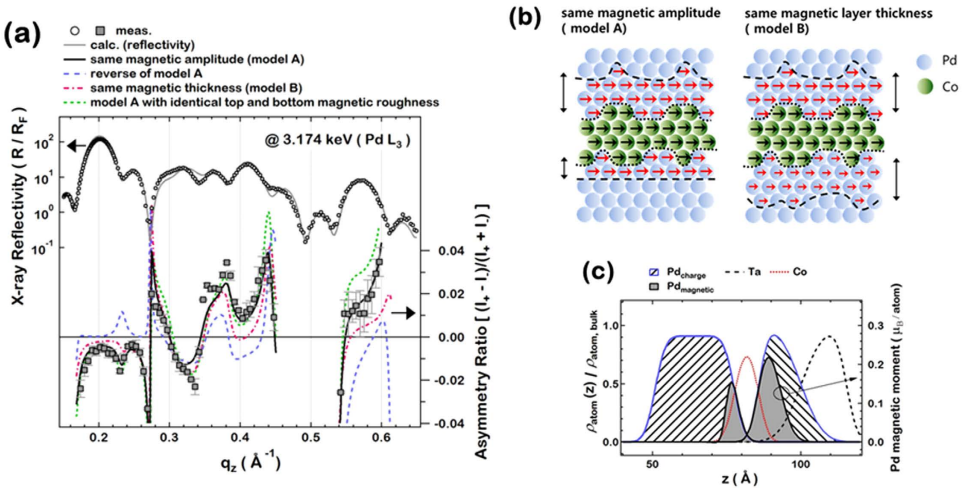

Figure 5. (**a**) Asymmetry ratios (bottom panel), which is defined as $(I_+ - I_-)/(I_+ + I_-)$ and sensitive to the magnetic moments, and the structure sensitive x-ray reflectivity (top panel) measured at the Pd L_3 edge. In the bottom panel, the solid line represents the best fit with model A and the other lines are the calculations with various models. (**b**) Depiction of the magnetic proximity effect of the Pd/Co/Pd system. The top and bottom Pd each have magnetic and nonmagnetic regions. (**c**) Density profiles normalized by the bulk value. The spatial extent of the magnetic region and the total magnetic moment (gray area) is greater for the top Pd. Note that Ta atoms significantly diffuse into the Pd layer on top of the Co layer and overlap the induced Pd magnetic layer.

Another possibility on why the top Pd has a larger total magnetic moment than the bottom Pd is the difference in structural properties of the top and bottom Pd layers. It is natural that the Pd film deposited on the Ta buffer (bottom Pd) and the Pd film deposited on the Co film (top Pd) have different structural properties (e.g. lattice constant, strain). Typically, energy band narrowing occurs when the lattice constant increases. Theoretical calculations predict that an increase in lattice constant could result in a magnetic moment in Pd due to an increase in 4*d* DOS near the Fermi level[52,53], while experimental studies show strain induced ferromagnetism in Pd nanoparticles[54]. Then, the thicker top Pd magnetic region in our analysis could indicate that the top Pd has a larger extent of the strained region. Earlier studies on Pd/Co multilayers show that indeed the strained region is larger for the Pd on top of Co[55]. The imperfect crystallinity of our film, evidenced by the dark regions in the HRTEM images in Fig. 2, prevents quantifying structural properties such as the lattice constant or strain. For an in depth structural analysis to distinguish the structure of the top and bottom Pd, a Pd/Co/Pd film with better epitaxial quality, possibly deposited by molecular beam epitaxy (MBE), might be needed. It should be noted that the nearly identical interfacial roughness at the bottom Pd/Co and top Co/Pd interfaces, as discussed earlier with the RXR results, suggests there is no significant difference between the intermixing at the top and bottom Co-Pd interfaces. This eliminates the possibility that a difference in inter-diffusion at the top and bottom Co-Pd interfaces is the origin of the difference in the magnetic proximity effect of Pd.

Any difference in the interfacial structural or magnetic properties greatly influences the spin transport properties in NM/FM/NM systems. For instance, in a Pd/Co/Pd multilayer system, a nonzero spin-orbit field was argued to result from a dissimilar Pd structure on top of and under the Co film[40]. Likewise the different interface structure between the Pt/Co and Co/Pt was used to explain the sizeable difference in the DMI[22]. In addition, the magnetic proximity effect is known to lead to modifications to spin transport phenomena such as increased resistivity, reduced SHE, and increased domain wall velocity[25,32,34]. Since the magnetic proximity effect is a consequence of the 3*d*–4*d* or 3*d*–5*d* hybridization, it is conceivable that spin transport properties in NM-FM systems, which is sensitive to the interfacial spin orbit coupling, is largely affected by the magnetic proximity effect. Therefore, the asymmetry in the induced magnetic moments should be considered in analysis of the interfacial transport properties. Moreover, the difference in the induced magnetic region of NM/FM and that of FM/NM can be utilized for engineering the spin dependent transport phenomena in spin-orbitronic devices. For example, nonmagnetic materials such as Pd or Pt could be intentionally inserted below or on top of the FM layer in order to enhance or reduce the resistivity, the SHE, the DMI, etc.

In summary, our experiments and analyses provide direct proof that there is indeed significant asymmetry in the interfacial magnetic properties, such as the total induced magnetic moment and magnetic thickness, between the top and bottom nonmagnetic layers in a NM/FM/NM structure, albeit little difference in the interfacial roughness at the two NM-FM interfaces. Further investigation on its exact physical origin, along with its implications on spin transport properties will help us understand the asymmetrical magnetic proximity effect we find in this study.

Methods

Thin film samples were deposited on a Si/SiO_2 substrate by dc magnetron sputtering. The base pressure was 1×10^{-8} Torr. The microstructure and elemental distribution of Pd/Co/Pd were measured by high resolution transmission electron microscopy (HRTEM), scanning transmission electron microscopy (STEM), and

energy-dispersive x-ray (EDX) spectroscopy performed on the cross sectional plane of Pd/Co/Pd using TITAN S 80–300 operated at 300 kV. The x-ray measurements (XMCD, XRMR) were performed at the Advanced Photon Source beamline 4-ID-D. All the experiments were performed at room temperature.

References

1. Miron, I. M. *et al.* Current-drven spin torque induced by the Rashba effect in a ferromagnetic metal layer. *Nat. Mater*. **9,** 230–234 (2010).
2. Miron, I. M. *et al.* Fast current-induced domain-wall motion controlled by the Rashba effect. *Nat. Mater*. **10,** 419–423 (2011).
3. Miron, I. M. *et al.* Perpendicular switching of a single ferromagnetic layer induced by in-plane current injection. *Nature* **476,** 189–193 (2011).
4. Ando, K. *et al.* Electric manipulation of spin relaxation using the spin-hall effect. *Phys. Rev. Lett*. **101,** 036601 (2008).
5. Kim, J. *et al.* Layer thickness dependence of the current-induced effective field vector in Ta|CoFeB|MgO. *Nat. Mater.* **12,** 240–245 (2013).
6. Fan, X. *et al.* Observation of the nonlocal spin-orbital effective field. *Nat. Commun*. **4,** 1799 (2013).
7. Liu, L., Lee, O. J., Gudmundsen, T. J., Ralph, D. C. & Buhrman, R. A. Current-induced switching of perpendicularly magnetized magnetic layers using spin torque from the spin hall effect. *Phys. Rev. Lett*. **109,** 096602 (2012).
8. Liu, L. *et al.* Spin-torque switching with the giant spin hall effect of tantalum. *Science* **336,** 555–558 (2012).
9. Ryu, K.-S., Thomas, L., Yang, S.-H. & Parkin, S. Chiral spin torque at magnetic domain walls. *Nat. Nanotechnol*. **8,** 527–533 (2013).
10. Emori, S., Bauer, U., Ahn, S.-M., Martinez, E. & Beach, G. S. D. Current-driven dynamics of chiral ferromagnetic domain walls. *Nat. Mater*. **12,** 611–616 (2013).
11. Kim, K.-W., Seo, S.-M., Ryu, J., Lee, K.-J. & Lee, H.-W. Magnetization dynamics induced by in-plane currents in ultrathin magnetic nanostructures with Rashba spin-orbit coupling. *Phys. Rev. B* **85,** 180404(R) (2012).
12. Pi, U. H. *et al.* Tilting of the spin orientation induced by Rashba effect in ferromagnetic metal layer. *Appl. Phys. Lett*. **97,** 162507 (2010).
13. Kim, K.-W., Moon, J.-H., Lee, K.-J. & Lee, H.-W. Prediction of giant spin motive force due to Rashba spin-orbit coupling. *Phys. Rev. Lett*. **108,** 217202 (2012).
14. D'Yakonov, M. I. & Perel, V. I. Current-induced spin orientation of electrons in semiconductors. *Phys. Lett. A*. **35,** 459–460 (1971).
15. Hirsch, J. E. Spin hall effect. *Phys. Rev. Lett*. **83,** 1834 (1999).
16. Zhang, S. Spin Hall effect in the presence of spin diffusion. *Phys. Rev. Lett*. **85,** 393 (2000).
17. Kato, Y. K., Myers, R. C., Gossard, A. C. & Awschalom, D. D. Observation of the spin hall effect in semiconductors. *Science* **306,** 1910–1913 (2004).
18. Wunderlich, J., Kaestner, B., Sinova, J. & Jungwirth, T. Experimental observation of the spin-Hall effect in a two-dimensional spin-orbit coupled semiconductor system. *Phys. Rev. Lett*. **94,** 047204 (2005).
19. Guo, G. Y., Murakami, S., Chen, T.-W. & Nagaosa, N. Intrinsic spin Hall effect in Platinum: First-principles calculations. *Phys. Rev. Lett*. **100,** 096401 (2008).
20. Dzyaloshinskii, I. E. Thermodynamical theory of weak ferromagnetism in antiferromagnetic substances. *Sov. Phys. JETP* **5,** 1259–1272 (1957).
21. Moriya, T. Anisotropic superexchange interaction and weak ferromagnetism. *Phys. Rev.* **120,** 91 (1960).
22. Je, S.-G. *et al.* Asymmetric magnetic domain-wall motion by the Dzyaloshinskii-Moriya interaction. *Phys. Rev. B* **88,** 214401 (2013).
23. Thiaville, A., Rohart, S., Jue, E., Cros, V. & Fert, A. Dynamics of Dzyaloshinskii domain walls in ultrathin magnetic films. *Europhys. Lett*. **100,** 57002 (2012).
24. Khvalkovskiy, A. V. *et al.* Matching domain wall configuration and spin-orbit torques for very efficient domain-wall motion. *Phys. Rev. B* **87,** 020402(R) (2013).
25. Ryu, K.-S., Yang, S.-H., Thomas, L. & Parkin, S. P. Chiral spin torque arising from proximity induced magnetization. *Nat. Commun*. **5,** 3910 (2014).
26. Bergmann, G. Transition from Pauli paramagnetism to band ferromagnetism in very thin Ni films. *Phys. Rev. Lett*. **41,** 264 (1978).
27. Vogel, J. *et al.* Structure and magnetism of Pd in Pd/Fe multilayers studied by x-ray magnetic circular dichroism at the Pd $L_{2,3}$ edges. *Phys. Rev. B* **55,** 3663 (1997).
28. Antel, W. J. *et al.* Induced ferromagnetism and anisotropy of Pt layers in Fe/Pt(001) multilayers. *Phys. Rev. B* **60,** 12933 (1999).
29. Wilhelm, F. *et al.* Layer-resolved magnetic moments in Ni/Pt multilayers. *Phys. Rev. Lett*. **85,** 413 (2000).
30. Wilhelm, F. *et al.* Interface magnetism in 3d/5d multilayers probed by x-ray magnetic circular dichroism. *Phys. Status Solidi A* **196,** 33–36 (2003).
31. Huang, S. Y. *et al.* Transport magnetic proximity effects in platinum. *Phys. Rev. Lett*. **109,** 107204 (2012).
32. Lu, Y. M. *et al.* Pt magnetic polarization on Y3Fe5O12 and magnetotransport characteristics. *Phys. Rev. Lett*. **110,** 147207 (2013).
33. Hase, T. P. A. *et al.* Proximity effects on dimensionality and magnetic ordering in Pd/Fe/Pd trialyers. *Phys. Rev. B* **90,** 104403 (2014).
34. Zhang, W. *et al.* Reduced spin-Hall effects from magnetic proximity. *Phys. Rev. B* **91,** 115316 (2015).
35. Zhou, X. *et al.* Magnetotransport in metal/insulating-ferromagnet heterostructures: Spin Hall magnetoresistance or magnetic proximity effect. *Phys. Rev. B* **92,** 060402(R) (2015).
36. Huang, S. Y., Wang, W. G., Lee, S. F., Kwo, J. & Chien, C. L. Intrinsic spin-dependent thermal transport. *Phys. Rev. Lett*. **107,** 216604 (2011).
37. Qu, D., Huang, S. Y., Hu, J., Wu, R. Q. & Chien, C. L. Intrinsic spin seebeck effect in Au/YIG. *Phys. Rev. Lett*. **110,** 067206 (2013).
38. Miao, B. F., Huang, S. Y., Qu, D. & Chien, C. L. Physical origins of the new magnetoresistance in Pt/YIG. *Phys. Rev. Lett*. **112,** 236601 (2014).
39. Haney, P. M., Lee, H.-W., Lee, K.-J., Manchon, A. & Stiles, M. D. Current-induced torques and interfacial spin-orbit coupling. *Phys. Rev. B* **88,** 214417 (2013).
40. Jamali, M. *et al.* Spin-Orbit Torques in Co/Pd Multilayer Nanowires. *Phys. Rev. Lett*. **111,** 246602 (2013).
41. Carcia, P. F., Meinhaldt, A. D. & Suna, A. Perpendicular magnetic anisotropy in Pd/Co thin film layered structures. *Appl. Phys. Lett.* **47,** 178 (1985).
42. Engel, B. N., England, C. D., Leeuwen, R. A. V., Wiedmann, M. H. & Falco, M. Interface magnetic anisotropy in epitaxial superlattices. *Phys. Rev. Lett*. **67,** 1910 (1991).
43. Boeder, F. J. A. D., Kuiper, D., Donkersloot, H. C. & Hoving, W. A comparison of the magnetic anisotropy of [001] and [111] oriented Co/Pd multilayers. *Appl. Phys. A* **49,** 507–512 (1989).
44. Zeper, W. B., Greidanus, F. J. A. M., Carcia, P. F. & Fincher, C. R. Perpendicular magnetic anisotropy and magneto-optical kerr effect of vapor-deposited Co/Pt-layered structures. *J. Appl. Phys.* **65,** 4971 (1989).
45. Lee, C. H., Farrow, R. F. C., Lin, C. J., Marinero, E. E. & Chien, C. J. Molecular-beam-epitaxial growth and magnetic properties of Co-Pt superlattices oriented along the [001], [110], and [111] axes of Pt. *Phys. Rev. B* **42** 11384(R) (1990).
46. Materlik, G. & Sparks, C. J. In *Reso*n*an*t Ano*ma*lous *X-ray Scattering: Theory and Applications* (ed. Fischer, K.) (North Holland, 1994).
47. Lee, D. R. *et al.* X-ray resonant magnetic scattering from structurally and magnetically rough interfaces in multilayered systems. I. Specular reflectivity. *Phys. Rev. B* **68,** 224409 (2003).

48. Hannon, J. P., Trammell, G. T., Blume, M. & Gibbs, D. X-ray resonance exchange scattering. *Phys. Rev. Lett*. **61,** 1245 (1988).
49. Roy, S. *et al.* Evidence of modified ferromagnetism at a buried Permalloy/CoO interface at room temperature. *Phys. Rev. B* **75,** 014442 (2007).
50. Choi, Y., Lee, D. R., Freeland, J. W., Srajer G. & Metlushko, V. Layer-resolved study of magnetic interaction effects in heterostructure dot arrays. *Appl. Phys. Lett*. **88,** 112502 (2006).
51. Hong, S. C., Lee, J. I. & Wu, R. Ferromagnetism in Pd thin films induced by quantum well states. *Phys. Rev. B*. **75,** 172402 (2007).
52. Moruzzi, V. L. & Marcus, P. M. Magnetism in fcc rhodium and palladium. *Phys. Rev. B* **39,** 471 (1989).
53. Chen, H., Brener, N. E. & Callaway, J. Electronic structure, optical and magnetic properties of fcc palladium. *Phys. Rev. B* **40,** 1443 (1989).
54. Oba, Y., Sato, T. & Shinohara, T. Ferromagnetism induced by strains in Pd nanoparticles. *Phys. Rev. B* **78,** 224417 (2008).
55. Awano, H., Suzuki, Y., Katayama, T. & Itoh, A. *In situ* measurement of stress in Co/Cu, Co/Pd, and Co/Au compositionally modulated multilayer films. *J. Appl. Phys*. **68,** 4569 (1990).

Acknowledgements

This work was supported by the KIST Institutional Program (2E26380), the Pioneer Research Center Program (2011-0027905), and NRF grants 2010-0004614, 2013R1A1A2011326, 2014K2A1A2048433, and 2013R1A2000245 funded by the Korean Government (MSIP and MOE). Work at the Advanced Photon Source is supported by the U.S. Department of Energy, Office of Science under Grant No. DEAC02-06CH11357.

Author Contributions

J.W.C. and D.R.L. coordinated the study. K.M.S. and J.W.C. prepared the samples. D.-O.K., K.M.S., Y.S.C., J.W.C. and D.R.L. performed the x-ray experiments. D.-O.K. and D.R.L. performed the x-ray data analysis. B.-C.M. and J.-S.K. interpreted the data. All authors discussed the results and contributed to preparing the manuscript.

Additional Information

Supplementary information accompanies this paper at http://www.nature.com/srep

Competing financial interests: The authors declare no competing financial interests.

How to cite this article: Kim, D.-O. *et al.* Asymmetric magnetic proximity effect in a Pd/Co/Pd trilayer system. *Sci. Rep.* **6**, 25391; doi: 10.1038/srep25391 (2016).

This work is licensed under a Creative Commons Attribution 4.0 International License. The images or other third party material in this article are included in the article's Creative Commons license, unless indicated otherwise in the credit line; if the material is not included under the Creative Commons license, users will need to obtain permission from the license holder to reproduce the material. To view a copy of this license, visit http://creativecommons.org/licenses/by/4.0/

Supplementary information

Asymmetric magnetic proximity effect in a Pd/Co/Pd trilayer system

Dong-Ok Kim[1,2], Kyung Mee Song[2,3], Yongseong Choi[4], Byoung-Chul Min[2], Jae-Sung Kim[3], Jun Woo Choi[2,a)], Dong Ryeol Lee[1,b)]

[1]*Department of Physics, Soongsil University, Seoul 06978, Republic of Korea*

[2]*Center for Spintronics, Korea Institute of Science and Technology, Seoul 02792, Republic of Korea*

[3]*Department of Physics, Sookmyung Women's University, Seoul 04130, Republic of Korea*

[4]*Advanced Photon Source, Argonne National Laboratory, Argonne, Illinois 60439, USA*

a) junwoo@kist.re.kr

b) drlee@ssu.ac.kr

Resonant x-ray reflectivity

X-ray reflectivity is sensitive to the gradient of the x-ray refractive index along the surface normal direction (z direction) which is used to determine the laterally averaged depth profile. The x-ray refractive index *n(z,E)* is given by

$$n(z,E) = 1 - \frac{\lambda^2 r_e}{2\pi} \sum_i \rho_{\mathrm{atom},i}(z)\left[f_i'(E) + i\, f_i''(E)\right] \qquad (1)$$

where λ is x-ray wavelength, r_e is the classical electron radius, the summation is over constituent atoms, and ρ_{atom} is the atom number per unit volume (atomic density). $f' + i\, f''$ is the complex atomic scattering factor, whose imaginary part is related to x-ray absorption, and the real part is related to the imaginary part by the Kramers-Kronig dispersion relation. The x-ray reflectivity intensities measured at grazing incidence angles can be calculated explicitly using the Parratt's recursive formalism[1] , which is an extension of optics theory to x-rays, with additional modification assuming a Gaussian distributed interfacial roughness. A Debye-Waller factor like form derived in the distorted wave Born approximation (DWBA) has been widely used[2].

Figure S1 shows the atomic scattering factors of the Pd atoms in Pd/Co/Pd near the Pd L_3 edge. The imaginary scattering factor f'' was obtained from the measured XAS data (Fig. 4(a)), which was then transformed into the real part f' using the Kramers-Kronig relation[3]. Both procedures use tabulated factors from away from the absorption edge for scaling (normalization)[4]. Since other constituent elements' scattering factors are almost constant, any change in reflectivity intensities at and away from the Pd L_3 edge results from the contrast in refractive indices at the Pd-Co and Pd-Ta interfaces. The vertical bars (blue) in Fig. S1 indicates that the contrast between the atomic scattering factors of Pd and Co atoms is

remarkably enhanced at the Pd L_3 edge (E = 3.174 keV) when compared with those away from the edge (E = 3.160 keV). This energy dependent contrast results in a clear difference between the x-ray reflectivity curves measured at the two energies near the Pd L_3 edge, as shown in Fig. 3(a).

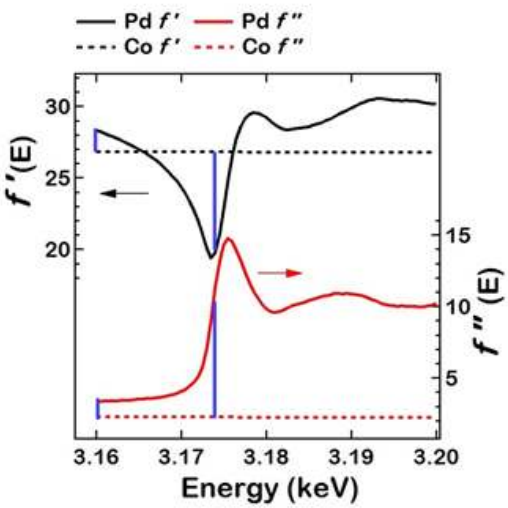

Figure S1. Atomic factors of the Pd atoms in Pd/Co/Pd near the Pd L_3 edge.

X-ray reflectivity fitting

For simultaneous fitting of the two x-ray reflectivity curves in Fig. 3(a), an identical set of structural parameters are used. This is due to the fact that only a noticeable difference in the physical parameters describing the two reflectivity curves at the different x-ray energies is the Pd atomic scattering factors. Considering the Gaussian distributed interface profiles assumed in the DWBA, the total refractive index profile can be calculated using an error function, the derivative of which is a Gaussian function. Figure 3(b) shows the total refractive index profiles, explicitly $\rho_{atom}(z) \cdot f'(\mathrm{E}, \mathrm{z})$, for the two different energies determined

from the best fit structure. Since the difference between two profiles (dash-dotted blue lines) only results from different atomic factors of Pd layers, it determines an element-specific depth profile of the Pd layers, which corresponds to

$$\rho_{\text{atom, Pd}}(z)\cdot\left[f'_{\text{Pd}}(3.16\,\text{keV})-f'_{\text{Pd}}(3.174\,\text{keV})\right]$$

X-ray resonant magnetic reflectivity

Similar to conventional x-reflectivity, x-ray resonant magnetic reflectivity is sensitive to the gradient of x-ray refractive index originating from the magnetic response. Typically the magnetic response in the x-ray refractive index is too small to be measurable, but it can be enhanced and observable when the incident x-rays are circularly polarized and the x-ray energy is tuned to the absorption edge of a specific magnetic element. Therefore, XRMR can determine laterally averaged depth profile of element-specific magnetic moments. Following Ref. 5, the magnetically sensitive part component is added to the complex x-ray atomic scattering factors for the magnetic element atoms. Then the atomic scattering factor in eq. (1) is given as

$$f'_{tot}(E)+i\,f''_{tot}(E)=\left(\hat{e}^*_f\cdot\hat{e}_i\right)\left[f'_c(E)+i\,f''_c(E)\right]+i\left(\hat{e}^*_f\times\hat{e}_i\right)\cdot\hat{m}(z)\left[f'_m(E)+i\,f''_m(E)\right] \qquad (2)$$

where $\hat{e}_{i(f)}$ and $\hat{m}$ are unit vectors of the incident(outgoing) x-ray polarization and magnetization of the magnetic layers, respectively. The magnetic atomic factors f'_m and factors f''_m are only detectable near the absorption edges of magnetic elements. Figure S2 shows the Pd magnetic atomic factor $f''_m(E)$ obtained from the measured XMCD in Fig. 4(a) with the same scaling factor used for the charge atomic factor $f''(E)$. The real part f'_m was obtained using the Kramers-Kronig relation.

Since the magnetic atomic factors are typically obtained from XMCD results, a homogeneous magnetization is assumed inside the magnetic layer, since XMCD is a bulk sensitive measurement. However, since Pd atoms are only magnetized near the Pd-Co interfaces, we added a factor $r(z)$ with a relative spatial distribution to the magnetic atomic factors as $i\left(\hat{e}_f^* \times \hat{e}_i\right) \cdot \hat{x}\, r(z) \left[f_m'(E) + i\, f_m''(E)\right]$. Since only the saturation magnetization is of interest, it is assumed that $\hat{m}(z) = \hat{x}$, which is along the x-ray beam direction in the sample surface plane.

To consider explicitly the polarization dependence of magnetic atomic factors in eq. (2), a full dynamical formalism or optical formula extended for polarized x-rays and resonant scattering amplitudes should be used[6]. However, a more realistic model with both structurally and magnetically rough interfaces can be taken into account in the DWBA formula. The magnetic DWBA formula can be simplified for circularly polarized x-rays in an approximation of grazing incidence angles, relatively weak resonant scattering amplitudes, and dominant magnetization along the beam direction in the sample surface plane[7]. Since our experimental conditions meet this approximation, we have used the simplified DWBA formula to explain quantitatively the magnetic depth profile of induced Pd magnetic moments. As in RXR, we assume a Gaussian distributed interfacial roughness in the DWBA formula used for the XRMR analysis to obtain the relative magnetic depth profile shown as the shaded area in Fig. 5(c).

.

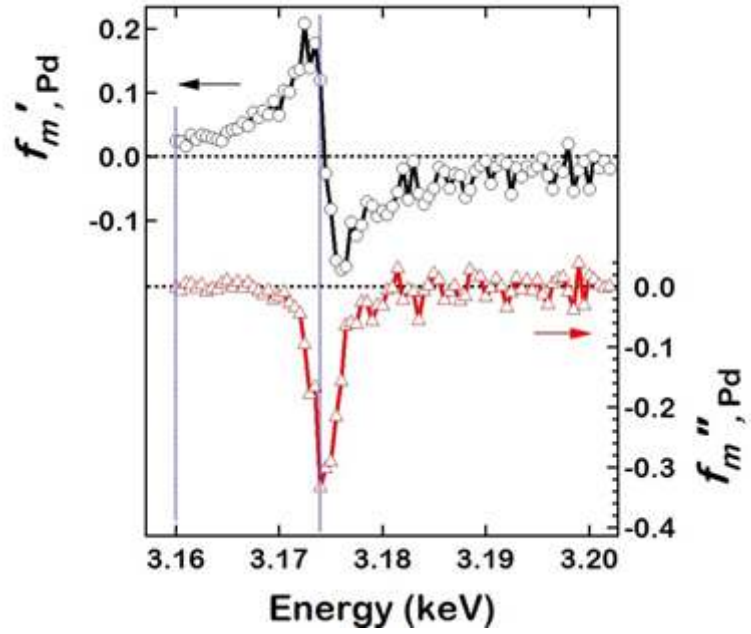

Figure S2. Magnetic atomic factors of the Pd atoms in Pd/Co/Pd near the Pd L_3 edge.

X-ray resonant magnetic reflectivity fitting with various models

To verify the validity of the asymmetric magnetic roughnesses determined from the best fit, we plot the calculated asymmetry ratios (green dotted lines in Fig. 5(a)) with identical magnetic roughness (1.5Å) at the top and bottom nonmagnetic Pd-magnetic Pd interface and other parameters unchanged. The green dotted line shows a clear deviation from the experimental data at high q_z's. Additionally, the calculated asymmetry ratio for the reverse case in which the parameters of the magnetic layers used for the best fit are switched for the top and bottom Pd layers ($d_{mag}^{top} < d_{mag}^{bot}$), is shown as the dashed blue lines in Fig. 5(b). The deviation from the measured data is obvious, in particular the reversed sign of the asymmetry ratio near $q_z \sim 0.23$ Å^{-1}. Finally, the calculated asymmetry ratio based on the best fit using model B (symmetric magnetic thicknesses but asymmetric magnetic amplitude) are shown as

the red dash-dotted lines in Fig. 5(a). The deviation from the experimental data is clear at high q_z's. It should be noted that this deviation is not improved by varying the fitting parameters. Since the magnetic moments of Pd induced by the Co atoms should result from the Pd 4*d*-Co 3*d* hybridization, the nearly identical chemical (electronic) structures at the Pd/Co and Co/Pd interfaces from the RXR analysis (Fig. 3) suggest that the induced magnetic moment per Pd atom should be similar between the top and bottom Pd films. Then it is plausible that, model A, with identical magnetic amplitudes $m_{\mathrm{Pd}}^{\mathrm{top}} = m_{\mathrm{Pd}}^{\mathrm{bot}}$ but different magnetic layer thicknesses $d_{mag}^{top} \neq d_{mag}^{bot}$, is more valid for explaining the measured asymmetry ratio.

Estimation of Pd magnetic moment

The lack of XMCD data at Pd L_2 edge prevents us from quantifying the Pd induced magnetic moment using the sum rule. According to Bailey *et. al.* , it can be estimated that a maximum Pd XMCD signal of -10 % (normalized by the step height at the Pd L_3 edge) correspond to a total magnetic moment of 0.116μ_B/atom[8]. Then a maximum XMCD signal of -4.7 %, as shown in Fig. 4(a), would correspond to 0.05μ_B/atom. The difference in the Pd moments is possibly due to the fact that there is some inaccuracy in the Pd magnetic moment values deduced from XMCD data in earlier studies, since the exact magnetic thickness is unclear. To estimate the absolute value of induced Pd magnetic moments, the following relationship between the XMCD and XRMR results should be considered:

$$m_{\mathrm{tot,Pd}} = \overline{m}_{\mathrm{Pd,\,XMCD}} \int \rho_{\mathrm{atom,Pd}}(z)\,dz = \overline{m}_{\mathrm{Pd,\,XRMR}} \int \rho_{\mathrm{atom,Pd}}(z)\; r(z)\,dz \qquad (3)$$

where $\overline{m}_{\mathrm{Pd,\,XMCD}}$ and $\overline{m}_{\mathrm{Pd,\,XRMR}}$ are the average magnetic moments for the XMCD and

XRMR data, respectively. The magnetic depth profile r(z) was determined from the best fit using a model where each induced magnetic layer has same magnetic moment within the layer and different magnetically rough interfaces. From Eq. (3), the corrected magnitude of the Pd magnetic moments, $\overline{m}_{\mathrm{Pd,\,XRMR}}$, is estimated to be 0.3$\mu_B$/atom. This magnitude is consistent with the result of Vogel *et. al.* for a 0.7 nm thick Pd in between Fe layers, where the Pd layers were assumed to be fully magnetized[9]. It should also be noted that the calculated induced Pd magnetic moment in Fe/Pd(001) was found to be 0.36~0.38μ_B/atom within two layers from the Fe-Pd interface[10]. The distribution of the induced Pd magnetic moments in Fig. 5(c) is plotted in units of μ_B/atom calculated by $\overline{m}_{\mathrm{Pd,\,XRMR}} \cdot r(z)$.

REFERENCES

1. Parratt, L. G. Surface studies of solids by total reflection of X-rays. *Phys. Rev.* **95**, 359 (1954).

2. Sinha, S. K., Sirota, E. B., Garoff, S. & Stanley, H. B. X-ray and neutron scattering from rough surfaces. *Phys. Rev. B* **38**, 2297 (1988).

3. Cross, J. O. *et al*. Inclusion of local structure effects in theoretical x-ray resonant scattering amplitudes using *ab initio* x-ray absorption spectra calculations. *Phys. Rev. B* **58**, 11215 (1998).

4. Henke, B. L., Gulikson, E. M. & Davis, J. C. X-ray interaction: Photoabsorption, scattering, transmission, and reflection at E=50-30,000 eV, Z=1-92. *At. Data Nucl. Data Tables* **54**, 181 (1993).

5. Hannon, J. P., Trammell, G. T., Blume, M. & Gibbs, D. X-ray resonance exchange scattering. *Phys. Rev. Lett.* **61**, 1245 (1988).

6. Stepanov, S. A. & Sinha, S. K. X-ray resonant reflection from magnetic multilayers: Recursion matrix algorithm. *Phys. Rev. B* **61**, 15302 (2000).

7. Lee, D. R. *et al*. X-ray resonant magnetic scattering from structurally and magnetically rough interfaces in multilayered systems. I. Specular reflectivity. *Phys. Rev. B* **68**, 224409 (2003).

8. Bailey, W. E. *et al*. Pd magnetism induced by indirect interlayer exchange coupling. *Phys. Rev. B* **86**, 144403 (2012).

9. Vogel, J. *et al*. Structure and magnetism of Pd in Pd/Fe multilayers studied by x-ray magnetic circular dichroism at the Pd $L_{2,3}$ sedges. *Phys. Rev. B* **55**, 3663 (1997).

10. Lee, S.-K. *et al*. Surface alloying and magnetism of ultrathin Fe films on Pd (001). *Phys. Rev. B* **65**, 014423 (2001).